Phonon gas: A lattice Boltzmann description

R. A. Guyer
Department of Physics and Astronomy, University of Massachusetts, Amherst, Massachusetts 01003
(Received 14 June 1993; revised manuscript received 22 April 1994)

A lattice Boltzmann computational scheme is developed and applied to a model of the phonon gas. This model has two types of phonons, transverse and longitudinal, that interact with one another through a three-phonon collision process. Exact and relaxation time approximation treatments of the collision operator are described. The computational scheme is tested in a study of the propagation of small-amplitude second sound where the predictions of linearized phonon hydrodynamics are confirmed. It is then employed to study two problems of current interest in nonlinear phonon hydrodynamics: (1) the propagation of linear second sound in the presence of a steady heat current, and (2) the propagation of nonlinear second sound.

PACS number(s): 51.10.+y, 51.30.+i, 63.20.Hp, 72.20.Ht

I. INTRODUCTION

The phonon gas was studied intensely about 25 years ago in the context of discussion of the connection between the microscopic description of a system and its hydrodynamics [1]. A substantial and varied body of theoretical work showed how to start with the Hamiltonian for an anharmonic crystal and end up with a hydrodynamics for the phonon gas [2]. This hydrodynamic supported a second-sound mode, i.e., the propagation of temperature fluctuations as waves. Experimental attempts to observe second sound in crystals proceeded apace, culminating in the initial observation of this phenomenon by Ackerman and co-workers [3] in helium crystals.

The experimental investigation of the behavior of a phonon gas is far more difficult than their theoretical elaboration because of the practical difficulty of having isotopic and/or chemical impurity free, single crystals of substantial size [3–5]. As of this writing there are perhaps four crystals in which phonon hydrodynamic behavior has been observed [6].

Recently there have been a number of theoretical investigations of the nonlinear behavior of the phonon gas. (The earlier work was devoted exclusively to the linear response of this gas.) The phenomena being described have their source in nonlinear hydrodynamic equations that are developed from the application of various general principles. The work of Coleman and co-workers [7], that leads, for example, to an unusual prediction about the behavior of second sound in the presence of a heat current employs the Cattaneo equation [8]. The work of Ruggeri and co-workers [9], on the behavior of large-amplitude temperature waves, is developed from a nonlinear hydrodynamics that is grounded in the modern extended thermodynamics.

It is of interest to have experiments to investigate the phonon gas phenomena that are predicted by these nonlinear phenomenologies and to have the ready means to interface experiment and phenomenology. The purpose of this paper is to develop these means. To this end we construct a lattice Boltzmann computational apparatus (LBA) for the phonon gas that is faithful to its known linear hydrodynamics. We use this computational apparatus to do experiments on the phonon gas that probe it beyond linear response where the nonlinear phenomenology has something to say.

Lattice Boltzmann models are computational schemes designed for the study of complex systems. The fundamental idea is that of developing computational rules for the microscopic behavior of a "fluid" that are as simple as possible while capturing the essential physics. These rules are used to study the behavior of the "fluid" in complex circumstances. Simple computational rules are called for because the bulk of computational effort is devoted to watching the influence of complex circumstances on the behavior of the fluid.

Notable examples of this line of research are the models of the Navier-Stokes fluid that have been developed and employed to study flow in porous media. These are described, for example, in the workshop proceedings edited by Doolen [10]. The phonon gas as we will encounter it here does not have the complexity of being in a pore space. It has intrinsic complexity in its microscopic structure. It is a fluid of two interpenetrating components, the longitudinal and transverse phonons, that convert one into the other. The phonon gas can be subject to external fields that couple strongly to its hydrodynamic variables or drive it well beyond the range of linear response.

In Sec. II we set up computational rules for a lattice Boltzmann model of a phonon gas that has two types of phonons, transverse and longitudinal, that interact with one another through cubic anharmonicity. That is, we adopt a three-phonon collision rule in which pairs of transverse phonons coalesce into a longitudinal phonon and vice versa. This collision process conserves energy and momentum but not "particle" number. Fundamental to going ahead with use of the computational rules are the analytic calculations that establish that the computational rules lead to the known physics in suitable circumstance. We sketch these calculations in Sec. III,

where we demonstrate that energy and momentum conservation laws for slowly varying long wavelength disturbances are the known equations of phonon hydrodynamics. As part of this demonstration we have to deal with a shortcoming of the exact (or linearized) three-phonon collision operator. It has a defective null space. We discuss this shortcoming (it is endemic to lattice Boltzmann formulations) for phonon systems. We circumvent it by employing a relaxation time approximation to the three-phonon collision operator. Thus (1) the equations of phonon hydrodynamics are found in the relaxation time approximation to the collision operator and (2) the three-phonon collision operator in the computational rules is replaced by the relaxation time approximation.

In Sec. IV we show the results of a series of numerical experiments carried out using the lattice Boltzmann description of the phonon gas. We make two experimental tests to see that the phonon gas so described obeys the linearized phonon hydrodynamics.

(a) We study the propagation of weak energy disturbances and compare their behavior with the expectation from the linearized hydrodynamics for propagation as second sound [2,3].

(b) We compare details of the evolution of the structure of temperature pulses with our expectation of the influence of phonon viscosity [5].

These experiments show the lattice Boltzmann computational apparatus to reliably describe the hydrodynamic behavior of the phonon gas. The satisfactory outcome of these experiments gives us confidence in using the LBA to look at the phonon gas under extreme conditions.

(c) By controlling the phonon-phonon collision rate we look in detail at the collision process as it assembles an initial disturbance into a second sound pulse.

(d) We examine the motion of a temperature disturbance that drives the system far from linear response and we examine the influence of the phonon-phonon collision rate on the tendency of nonlinear disturbances to form shocks.

(e) We study the propagation of a weak energy disturbance in the presence of a steady heat current to look for the unusual behavior found from the nonlinear hydrodynamics of Coleman and co-workers [7]. (Coleman and co-workers predict that a temperature pulse will move faster against the direction of a heat current than it will with a heat current.)

We summarize our findings in Sec. V. Some details of the eigenvalue problem associated with the collision operator are found in Appendix A. Details associated with the conservation laws, the use of local equilibrium distribution functions, and the relaxation time approximation are found in Appendix B.

II. PHONONS

Consider a typical dielectric crystal (or liquid ^{4}He) at low temperature. The elementary excitations of the crystal are the thermally excited transverse and longitudinal phonons. Let us imagine that the crystal is perfect, without isotopic or other impurities, so that the fundamental interactions among the phonons are the three-phonon processes due to cubic anharmonicity. We wish to have a lattice Boltzmann description of this phonon gas that is faithful to its essential physics. For illustrative purposes we use a two dimensional example.

Take the space in which the phonon gas resides to be covered with hexagons as shown in Fig. 1(a). Each site is located with a vector $\mathbf{X}_{m,n}=m\mathbf{a}_1+n\mathbf{a}_2$. We denote these vector locations generically by $\mathbf{x}$. At each site there are 12 states for the phonons, six transverse states and six longitudinal states. We label these states by $\sigma=0,1$ for transverse and longitudinal and by $\mathbf{e}_1,\ldots,\mathbf{e}_6$, the directions of motion of the phonons. See Fig. 1(b).

The energies of the phonons in the six transverse (longitudinal) states are $\epsilon/2$ (ϵ). Both the six transverse and the six longitudinal phonons carry the same magnitude momentum $p=\hbar k$ in the six vector directions $\mathbf{e}_1,\ldots,\mathbf{e}_6$. As all of the phonons, both longitudinal and transverse, carry the same magnitude momentum but have energies differing by a factor of 2 we have $c_L/c_T=2$.

We describe the states of a site $\mathbf{x}$ at time t by specifying the 12 phonon distribution functions (more properly the expected number of phonons in the states) with

$$R(\mathbf{x},t;\epsilon_\sigma,\mathbf{e}_i)\,, \tag{1}$$

where $i=1,\ldots,6$, and $\epsilon_0=\epsilon/2$, and $\epsilon_1=\epsilon$.

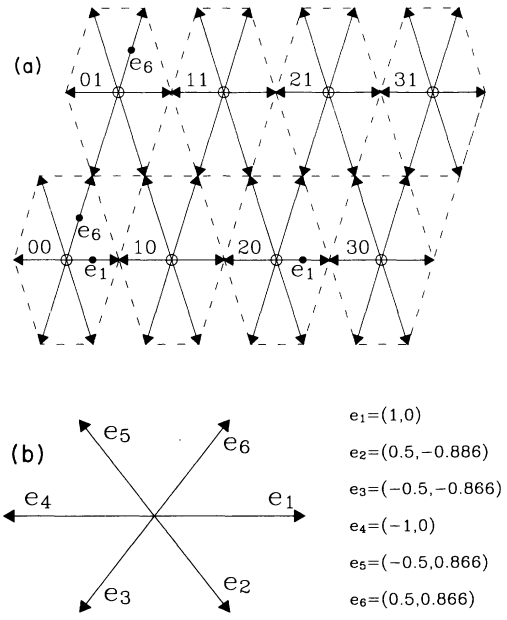

FIG. 1. Geometry. (a) The physical space is covered with hexagons (sites) that are denoted by the pair of integers that describe their location in terms of the vectors (1,0) and $(0.5,0.5\times\sqrt{3})$. There are six directions (states) for longitudinal and transverse phonon momentum at each site denoted by vectors $\mathbf{e}_1,\ldots,\mathbf{e}_6$. These vectors are shown in (b). In one time step the discrete translation operator carries the phonon distribution function for the state $\mathbf{e}_j$ at site $\mathbf{x}$ to the state $\mathbf{e}_j$ at site $\mathbf{x}+\mathbf{e}_j$ for a transverse phonon or to the state $\mathbf{e}_j$ at site $\mathbf{x}+2\mathbf{e}_j$ for a longitudinal phonon. This is illustrated in (a): the longitudinal phonons in state $\mathbf{e}_1$ at site (0,0) go to state $\mathbf{e}_1$ at site (2,0); the transverse phonons in state $\mathbf{e}_6$ at site (0,0) go to state $\mathbf{e}_6$ at site (0,1).

The lattice Boltzmann rule for time evolution of the system is a rule for the motion of the phonon distribution functions. We take this rule to be

$$T_{i\sigma}R(\mathbf{x},t;\epsilon_\sigma,\mathbf{e}_i)=R(\mathbf{x},t;\epsilon_\sigma,\mathbf{e}_i)+\left[\frac{\partial R(\mathbf{x},t;\epsilon_\sigma,\mathbf{e}_i)}{\partial t}\right]_{\text{collision}}, \quad (2)$$

where

$$T_{i\sigma}=\exp\left[\Delta t\frac{\partial}{\partial t}+a_\sigma\mathbf{e}_i\cdot\nabla\right]$$

is the space-time translation operator. Here $a_\sigma=a$ $(2a)$ for transverse (longitudinal) states; a is the distance between adjacent hexagon centers. The longitudinal phonons move twice as far as the transverse phonons in time Δt; see Fig. 1.

For the rate of change of $R(\mathbf{x},t)$ due to collision we take the collision operator appropriate to the three-phonon collision processes shown in Fig. 2; transverse:

$$\left[\frac{\partial R_i^0}{\partial t}\right]_c=W_i^0=w\Delta t[N_{i-1}(1+M_i)(1+M_{i-2})+N_{i+1}(1+M_i)(1+M_{i+2})-M_iM_{i-2}(1+N_{i-1})-M_iM_{i+2}(1+N_{i+1})], \quad (3)$$

longitudinal:

$$\left[\frac{\partial R_i^1}{\partial t}\right]_e=W_i^1=w\Delta t[M_{i+1}M_{i-1}(1+N_i)-N_i(1+M_{i+1})(1+M_{i-1})], \quad (4)$$

where w is a microscopic collision rate and the direction index is read modulo 6. [We adopt the following notation: R is a generic distribution function; when longitudinal and transverse distribution functions are explicitly exhibited in an equation we use M for transverse and N for longitudinal. Here M_i and N_i are shorthand for $M(1;\epsilon/2,\mathbf{e}_i)$ and $N(1;\epsilon,\mathbf{e}_i)$. It is sometimes useful to use R_i^σ; $R_i^0=M_i$ and $R_i^1=N_i$. A generic space-time point $(\mathbf{x},t)$ is denoted 1, $R(\mathbf{x},t)=R(1)$.] Equations (2)–(4) are a complete set of rules for time evolution of the phonon distribution function.

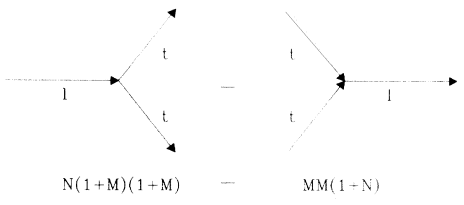

FIG. 2. Phonon collision processes. The cubic anharmonicity leads to three-phonon collision processes. Longitudinal phonons break up into two transverse phonons (on the left) or are created by two transverse phonons (on the right). The net rate of change of the number of longitudinal phonons is the difference between these two processes.

When the phonon gas at all sites is at ambient temperature characterized by β_0 it is in strict thermal equilibrium [11],

$$R_i^\sigma=\frac{1}{e^{\beta_0\epsilon_\sigma}-1}, \quad \forall i . \quad (5)$$

The phonon gas is in local thermal equilibrium when R^σ is given by

$$\bar{R}_i^\sigma(1)=\frac{1}{e^{\beta(1)[\epsilon_\sigma-p\mathbf{e}_i\cdot\mathbf{u}(1)]}-1} \quad \forall i , \quad (6)$$

where $\beta(1)$ is inverse of the temperature at 1 and $\mathbf{u}(1)$ is the drift velocity at 1. This distribution function is a local equilibrium distribution function in that if all of the phonon distribution functions for the states at a site have R^σ given by Eq. (5), with the same value of β and $\mathbf{u}$, the collision operator causes no rearrangement of the phonons among the states. The quantities $\beta(1)$ and $\mathbf{u}(1)$ are termed the *local equilibrium variables* as their values determine the local equilibrium distribution function.

For the strict equilibrium distribution function given by Eq. (5) or the local equilibrium distribution function given by Eq. (6) the collision operator causes no change. The collision operator operates independently at each site. The temperature and drift velocity at a site characterize the local equilibrium distribution function and therefore the energy and momentum at the site. Thus $\beta(1)$ and $\mathbf{u}(1)$, the local equilibrium variables, are suitable for description of the hydrodynamic modes of the phonon gas.

The computational rules exhibited above will be useful to us if we can establish that they capture the essential physics we believe is appropriate to the behavior of the system. This physics is referred to as phonon hydrodynamics. Demonstration that the appropriate hydrodynamic equations follow from the computational rules is the subject of Sec. III. To fix notation and prepare for Sec. III we describe several approximations to the computational rules.

(a) The Boltzmann approximation to the translation operator. We write

$$T_{i\sigma}-1\approx\Delta t\frac{\partial}{\partial t}+a_\sigma\mathbf{e}_i\cdot\nabla\equiv\Delta t\mathcal{L} . \quad (7)$$

The discrete translation of the computation rule approaches Boltzmann translation, $\mathcal{L}$, for $\Delta t\to 0, a_\sigma/\Delta t\to c_\sigma$.

(b) The linear approximation to the collision operator. We expand W_i^0 and W_i^1 in terms of the departure of R_i^σ away from strict thermal equilibrium. We use $\Delta M=M-P_0$ and $\Delta N=N-Q_0$ where $P_0=1/(e^{x/2}-1)$ and $Q_0=(1/e^x-1)$ to write

$$\frac{W_i^\sigma}{\Delta t}\equiv\sum_{j\sigma'}wA_{\sigma\sigma'}\Delta_{ij}^{\sigma\sigma'}\Delta R_j^{\sigma'} . \quad (8)$$

Here $\Delta R^0=\Delta M$, $\Delta R^1=\Delta N$,

$$\Delta_{ij}^{00}=\delta_{j,i+2}+2\delta_{j,i}+\delta_{j,i-2} ,$$

$$\Delta_{ij}^{01}=\Delta_{ij}^{10}=-(\delta_{j,i+1}+\delta_{j,i-1}) ,$$

$$\Delta_{ij}^{11}=\delta_{j,i} ,$$

$A_{11}=A_{01}=1+2P_0$, and $A_{10}=A_{00}=P_0-Q_0$.

(c) The relaxation time approximation to the collision operator. The collision operator is replaced by

$$-\frac{1}{\tau}[R(1;\epsilon_\sigma,\mathbf{e}_i)-\bar{R}(\beta(1),\mathbf{u}(1);\epsilon_\sigma,\mathbf{e}_i)] , \tag{9}$$

where $\bar{R}(\beta(1),\mathbf{u}(1);\epsilon_\sigma,\mathbf{e}_i)$ is a local equilibrium distribution function. It is characterized by $\beta(1),\mathbf{u}(1)$, the local equilibrium variables, that are found from the energy and momentum at site 1. Some details involved in carrying out this procedure are shown in Appendix B.

III. CONSERVATION LAWS

In this section we show that in suitable approximation to the lattice Boltzmann computational rules, Eqs. (2)–(4), the known hydrodynamic equations for the phonon gas are recovered. In making this demonstration we uncover the conditions that circumscribe the connection between the computational rules and physical behavior.

The hydrodynamic equations for a system describe its behavior for small fluctuations away from equilibrium that vary slowly in space and time. Thus we consider the computational rules using (a) the Boltzmann approximation to the displacement operator, Eq. (7), and (b) the linear approximation to the collision operator, Eq. (8). The linearized phonon Boltzmann equation is schematically

$$\mathcal{L}\Delta R(1)=-\mathcal{C}_L(1)\Delta R(1) , \tag{10}$$

where we have explicitly inserted the argument $1=\mathbf{x},t$ to emphasize that the collision operator operates on the phonons at a site. It is from analysis of this equation that we derive the hydrodynamic equations.

Treatment of Eq. (10) initially focuses on the collision operator, Eq. (8). Because $A_{01}\neq A_{10}$ it is not symmetric in $i\sigma\leftrightarrow j\sigma'$. It is made symmetric by using $r^\sigma=\sqrt{A_{\sigma\sigma}}R^\sigma$, $\bar{r}^\sigma=\sqrt{A_{\sigma\sigma}}\bar{R}^\sigma$, and $\Delta r^\sigma=\sqrt{A_{\sigma\sigma}}\Delta R^\sigma$. Then

$$\mathcal{L}_{i\sigma}\Delta r_i^\sigma=-\sum_{j,\sigma'}\mathcal{C}_{ij}^{\sigma\sigma'}\Delta r_j^{\sigma'} , \tag{11}$$

where

$$\mathcal{C}_{ij}^{\sigma\sigma'}=wa_{\sigma\sigma'}\Delta_{ij}^{\sigma\sigma'} ,$$

$a_{00}=A_{00}$, $a_{01}=a_{10}=\sqrt{A_{00}A_{11}}$, and $a_{11}=A_{11}$. The virtue of this form of the equation of motion for the distribution function is that the collision operator $\mathcal{C}$ is a real symmetric operator. As such it defines an eigenvalue problem,

$$\mathcal{C}\eta_\nu=\lambda_\nu\eta_\nu ,$$

with desirable properties, e.g., a complete orthonormal set of states with a real non-negative eigenvalue spectrum. We use this complete set of states to study Eq. (11).

The most important properties of the eigenvalue problem defined by $\mathcal{C}$ follow from physical argument. Phonon distribution functions of the form of Eq. (6), in which the temperature and drift velocity are the same for all phonons at a site, are unchanged by the collision process. They are local equilibrium distribution functions. Thus these distribution functions can be constructed from vectors that reside in the null space of the collision operator. (The null space of $\mathcal{C}$ is the set of eigenvectors with eigenvalue zero.) The form of these vectors can be found from examination of the effect of the collision operator on the local equilibrium distribution function. We find them by this method in Appendix A. They are

$$\eta_0(\epsilon_\sigma,\mathbf{e}_i)=C_0\left[\frac{\epsilon}{2\sqrt{A_{00}}}\delta_{\sigma,0}+\frac{\epsilon}{\sqrt{A_{11}}}\delta_{\sigma,1}\right] , \tag{12}$$

$$\eta_{1\gamma}(\epsilon_\sigma,\mathbf{e}_i)=C_1(\mathbf{e}_i)_\gamma\left[\frac{1}{\sqrt{A_{00}}}\delta_{\sigma,0}+\frac{1}{\sqrt{A_{11}}}\delta_{\sigma,1}\right] ,$$

$$\gamma=x,y ; \tag{13}$$

C_0 and C_1 are normalization constants. The local equilibrium distribution function is a function of the local value of the temperature, $\beta_0+\delta\beta(1)$, and the drift velocity, $\mathbf{u}(1)$. It is able to be expressed as a function of the vectors η_0, η_{1x}, and η_{1y} that reside in the null space, and of the hydrodynamic variables, in the form

$$\Delta\bar{r}(1)=A_0(1)|0\rangle+\sum_{\beta=1,2}A_\beta(1)|\beta\rangle , \tag{14}$$

where $A(1)$ is shorthand for $A(\beta(1),\mathbf{u}(1))$. Here we use the notation $\eta_0=|0\rangle$, $\eta_{1\gamma}=|1\gamma\rangle$. The amplitudes $A_0(1)$, $A_\beta(1)$ are functions of the local equilibrium variables. In linear approximation to the departure of $\Delta\bar{r}$ from strict equilibrium $A_0(1)\propto\delta\beta(1)$ and $A_{1\gamma}(1)\propto u_\gamma(1)$. To nonlinear order in $\delta\beta(1)$ and $\mathbf{v}(1)$ the amplitudes, A_0 and A_β, are more complicated functions of the local equilibrium variables. An illustration of this is provided in Appendix B.

The physical quantities of interest in discussing the conservation laws and physical phenomena are the energy and momentum at each site in the system:

$$\Delta E(1)=\sum_{\sigma,i}\epsilon_\sigma\Delta R(1;\epsilon_\sigma,\mathbf{e}_i) , \tag{15}$$

$$\Delta P_\gamma(1)=\sum_{\sigma,i}p(\mathbf{e}_i)_\gamma\Delta R(1;\epsilon_\sigma,\mathbf{e}_i) . \tag{16}$$

Using $\Delta r^\sigma=\sqrt{A_{\sigma\sigma}}\Delta R^\sigma$ and comparison with Eqs. (12) and (13) shows that to within a numerical factor $\Delta E(1)$ and $\Delta P_\gamma(1)$ are found from projection of Δr onto the vectors $|0\rangle$ and $|1\gamma\rangle$. We define a scaled energy and momentum by

$$\Delta e(1)=\langle 0|\Delta r(1)\rangle , \tag{17}$$

$$\Delta p_\gamma(1)=\langle\gamma|\Delta r(1)\rangle . \tag{18}$$

We term $\Delta e(1)$ and $\Delta\mathbf{p}(1)$ the *hydrodynamic variables* of

the phonon gas. [In using this language we are making a distinction between the *hydrodynamic variables* and the *local equilibrium variables,* see below Eq. (6), that is important when we consider nonlinear phenomena. For linear disturbances $\delta\beta(1) \propto \Delta e(1)$ and $\mathbf{u}(1) \propto \Delta \mathbf{p}(1)$.]

The conservation laws are found by multiplying Eq. (10) by energy and momentum and summing as in Eqs. (15) and (16). We show in Appendix A that the eigenvalue problem involving the linearized three-phonon collision operator has a null space with six vectors. There are three vectors associated with energy and momentum, those given by Eqs. (12) and (13), and three vectors that represent highly nonuniform phonon density at a site. (Difficulties of this kind are well known in this context [10]). The problem is caused by the coarse graining of momentum space. Because of the geometry and $c_L/c_T=2$ there are pathological configurations of the phonons that have $\lambda=0$, i.e., that are not degraded by the three-phonon collision process. (We will see evidence for the existence of these phonon configurations in one of the illustrative numerical examples described in the next section.) Qualitatively similar nonuniform phonon densities are possible in the description of real phonon systems. However, in such systems the amount of momentum space for these nonuniform configurations is vanishingly small. Here the lattice Boltzmann coarse graining of momentum space has emphasized their presence. We can in principle "solve" this problem by introducing additional collision processes. Our concern is not simply with getting to the Navier-Stokes equation [10]. Thus we look to the Hamiltonian for guidance [2,12]. It admits (a) three-phonon processes that do not conserve momentum, the umklapp processes, (b) four-phonon processes, $l+t \rightarrow l+t$, and (c) higher order processes. All of these collision processes occur at rates that are controlled by the temperature. Thus as $T \rightarrow 0$, i.e., $w \rightarrow 0$, the umklapp processes, the four-phonon processes, etc. disappear relative to the three-phonon momentum conserving processes. As we wish to employ the LBA as $T \rightarrow 0$ the higher order phonon processes are not a valid "solution." To avoid these difficulties in the present context we replace the exact collision operator (or its linearized version) by a relaxation time approximation, Eq. (9).

The physical idea behind a relaxation time approximation is that at each moment of time, at each site $\mathbf{x}$ the phonons have total energy $e(\mathbf{x},t)$ and total momentum $\mathbf{p}(\mathbf{x},t)$. If the phonon distribution functions at $\mathbf{x}$ were given by the local equilibrium distribution function, Eq. (6), that gave rise to $e(\mathbf{x},t)$ and $\mathbf{p}(\mathbf{x},t)$, then the collision operator would cause no rearrangement of the phonons. It is departure of the phonon distribution functions from this local equilibrium distribution function that causes the collision process to work. Thus we write

$$\left[\frac{\partial R_{i\sigma}}{\partial t}\right]_c = -\frac{1}{\tau}[R(1,\mathbf{e}_i\sigma) - \bar{R}(1,\mathbf{e}_i\sigma)] \ . \tag{19}$$

The computation rules now become Eqs. (2) and (19).

Demonstration that this approximation treatment of the collision operator leads to the conservation laws is given, for example, in Guyer and Krumhansl. What one finds upon working out the conservation equations to leading order in the relaxation time (this means drop $\tau\mathcal{L}$ compared to 1) is the equations of hydrodynamics that are independent of transport coefficients. These are the terms with which we are principally concerned. [In Appendix B we work out the hydrodynamic equations to second order in the local equilibrium variables for the lattice Boltzmann description of the phonon system. The resulting equations are Eqs. (B14) and (B15). In Appendix B we also exhibit the hydrodynamic equations to second order in the hydrodynamic variables.] We do not describe details of finding the hydrodynamic equations to higher order in $\tau\mathcal{L}$. Their treatment, in relaxation time approximation and more elaborately, is also given by Guyer and Krumhansl. A Navier-Stokes equation for the phonon gas is found. We establish a Navier-Stokes equation for the phonon gas described by the LBA by doing a numerical experiment that looks at the evolution of the structure of a temperature pulse.

IV. RESULTS

In this section we describe the results of a series of numerical experiments on the behavior of a phonon gas carried out using the LBA described above. The first of these demonstrates that the system behaves as we expect. It shows behavior in agreement with linear hydrodynamics. We then explore the behavior of the phonon gas away from linear hydrodynamics.

The phonon system is taken to be the system described by the following computational rules.

(1) The discrete translation rule of Eq. (2).

(2) The relaxation time approximation to the collision operator, Eq. (9). [The local equilibrium distribution function required to implement Eq. (9) is determined by the procedure described in detail in Appendix B.] The parameters that characterize the ambient conditions of the phonon gas are described as follows.

(a) Strict equilibrium: $\beta=\beta_0, \mathbf{u}=0 \ \forall \mathbf{x}$, i.e., the ambient temperature of the phonon gas is uniform; it has no drift velocity. The phonon distribution function is the strict equilibrium distribution function of Eq. (5) that is unchanged by the collision operator.

(b) A choice of the phonon collision rate w. In practice this rate is a function of physical variables that describe impurities, dislocations, and other features of a particular phonon system under study. Here we are using the cubic anharmonicity, common to all systems, that depends on atomic forces at work between the atoms [12]. In the relaxation time approximation the rate for this process would be a function of temperature. To avoid dealing with particular models of the collision process we take w to be a parameter that we vary through values that correspond roughly to $T<\Theta_D/10$, where Θ_D is the Debye temperature.

(c) As matters of principle are involved we work in $d=2$ with disturbances that are one dimensional.

(d) We disturb the system away from its equilibrium state and observe the response.

Example 1. At $\beta_0=1, \mathbf{u}=\mathbf{0}, w=0.1$ we disturb the system at $x=0$ at $t=0$ with $\beta=0.9$, i.e., an energy pertur-

bation or temperature perturbation at the origin. (Here and throughout we use $\epsilon=1$ so that the values of β are really values of $\beta\epsilon$.) We show in Figs. 3(a) and 3(b) the energy perturbation, in units of the ambient temperature, i.e., $\beta_0\Delta e$ of Eq. (17), as a function of position at various times after $t=0$. The horizontal axis in these figures is a distance away from the location of the perturbation, $x=0$, in units of hexagons; it is the site number. Time is measured in units of Δt. [In one time unit a transverse phonon moves one hexagon unit (one site) and a longitudinal phonon moves two hexagon units (two sites) as in Fig. 1(a).] In Fig. 3(a) we show the results for $t=10$ and 25 time units and in Fig. 3(b) we show the results for $t=40$, 60, 80, and 100 time units. Let us begin by looking at Fig. 3(a) for the early time response. The initial disturbance creates transverse and longitudinal phonons at the origin that are out of thermal equilibrium. The collision rate, $w=0.1$, is quite low and we see that at early times the disturbance has not thermalized. For example, at $t=10$ there is an energy spike at $x=\pm 20$ corresponding to longitudinal phonons that are in ballistic flight away from the origin and have had no collisions. There are similar features at $x=\pm 10$ due to ballistic transverse phonons traveling in the $\pm x$ direction and ballistic longitudinal phonons traveling at $\pm 60°$ of the $\pm x$ axis. Even transverse phonons traveling at $\pm 60°$ of the $\pm x$ axis are seen at $x=\pm 5$. If we look at longer times, $t=25$, we see that these ballistic features have been degraded by collision. As this degradation proceeds, the background of scattered phonons increases. In this figure we have indicated with filled squares the location at which the energy perturbation would be found if it traveled as a hydrodynamic mode, i.e., a second-sound pulse. It is toward the locations appropriate to the hydrodynamic mode that the phonons are being driven by the collision process.

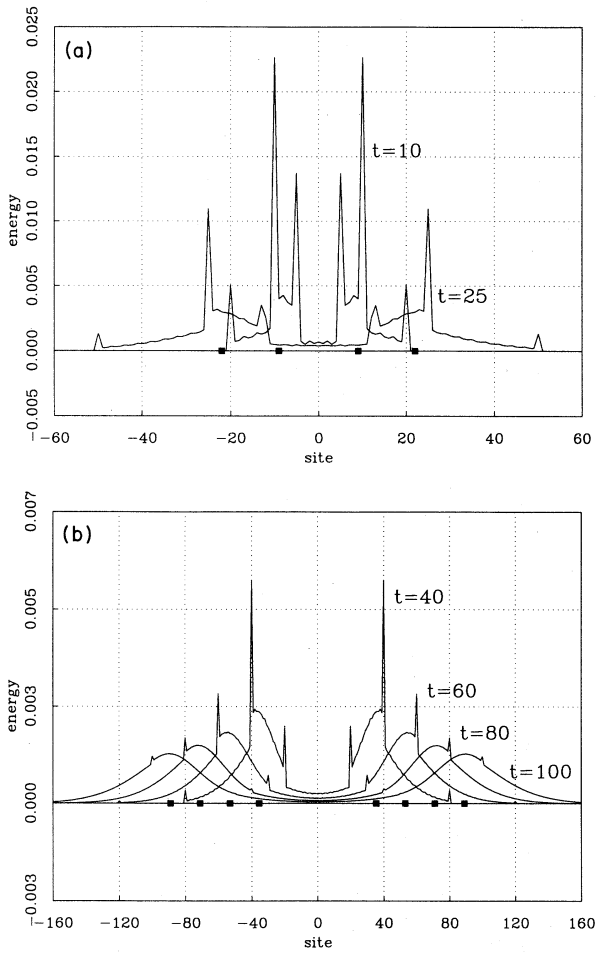

FIG. 3. Energy fluctuation as a function of position. For the conditions of example 1, $\beta_0=1, \beta=0.9, u=0, w=0.1$, the disturbance is at $\mathbf{x}=\mathbf{0}$ at $t=0$. (a) The energy fluctuation is plotted as a function of site number for $t=10$ and 25 time steps. (b) The energy fluctuation is plotted as a function of site number for $t=40$, 60, 80, and 100 time steps. The filled squares show the expected location of a second-sound pulse.

Upon looking at Fig. 3(b) we see that as time progresses ($t=40$, 60, 80, and 100) the collision process assembles the energy perturbation into the second-sound hydrodynamic mode. There are still some phonons that appear to be ballistic. (The choice $w=0.1$ was made so that there are a few such phonons to serve as a time marker.) The result expected from phonon hydrodynamics, Eq. (B16) from Appendix B, yields $c_2/c_L=0.443$ for $\beta_0=1$, where c_2 is the second-sound velocity. Thus at $t/\Delta t=M$ energy traveling as the second-sound mode should be at

$$\frac{x}{a}=0.886M \ .$$

It is this expected location for the energy fluctuation that is shown by filled boxes on the horizontal axis. The energy perturbation is traveling at the second-sound velocity.

As the energy perturbation moves further from the origin it decreases in amplitude and broadens. These phenomena are due to the finite rate of collision among the phonons or to terms in the hydrodynamics that are beyond the leading terms that follow from energy and momentum conservation. The hydrodynamic equations discussed above and worked out in Appendix B, Eqs. (B14) and (B15), have only the leading terms, those that do not involve the collision rate. Guyer and Krumhansl have worked out the hydrodynamics for a one component phonon gas (one polarization of phonon) to order $\tau\mathcal{L}\tau\mathcal{L}$. We will use their results to get an idea about the effects of collisions.

Guyer and Krumhansl find that the leading corrections to the equation for the energy current $\mathbf{Q}$ (essentially the momentum conservation law) lead to a Navier-Stokes-like equation of the form

$$\frac{\partial}{\partial t}\mathbf{Q}+\cdots=\cdots\eta[\nabla\cdot\nabla\mathbf{Q}+2\nabla\cdot(\nabla\cdot\mathbf{Q})] \ , \qquad (20)$$

where $\eta\propto c^2/w$ is a phonon viscosity. This term is responsible for Poiseuille flow of a phonon gas and in an energy or temperature pulse it is responsible for the phonons' random walking relative to the center of the moving pulse. Thus the temperature pulse should become broader as $\sqrt{t/w}$ and decrease in height as $\sqrt{w/t}$. We test this expectation for the behavior of the temperature pulse in example 2.

Example 2. At $\beta_0=1, \mathbf{u}=\mathbf{0}\ \forall \mathbf{x}$ we disturb the system at $x=0$ at $t=0$ with $\beta=0.9$. We look at the behavior of the energy perturbation for various collision rates and at various times. See Figs. 4(a)–4(c). As illustration of the influence of the strength of the collision rate we show in Fig. 4(a) the right hand going pulse at $t=40$ for values of the collision rate varying from 0.20 to 1.40. To show how an energy pulse spreads as time goes on we show, in Fig. 4(b), the right hand pulse for $w=0.20$ at $t=20,30,40,60,80,100$. To construct this figure from the data we have translated the energy pulses back toward the origin by [(second-sound velocity)×(time)] so that they overlap and the pulse spreading with the duration of flight will be apparent. From these and similar data we have measured the pulse height and pulse width. To test the expectation

$$(\text{height}) \propto \sqrt{w/t}\ , \tag{21}$$

$$(\text{width}) \propto \sqrt{t/w}\ , \tag{22}$$

we have plotted the measured height and width of the temperature pulses as a function of w/t in Fig. 4(c). (The scales in the figure are $\log_{10}$-$\log_{10}$.)

The data in this figure involve various values of w and t. It is apparent that $t/w \propto \eta t$ is a good variable for describing both the height and width of a temperature pulse. The solid lines in the figure are guides to the eye of slope $+\frac{1}{2}$ and $-\frac{1}{2}$. The expectations of Eqs. (21) and (22) are borne out.

We take the results of examples 1 and 2 to establish that the lattice Boltzmann model behaves as the linear hydrodynamics of the phonon gas would have it behave. It carries energy fluctuations as a second-sound mode. This mode is broadened by the viscous processes that operate like those described by a Navier-Stokes equation. This phonon gas would carry heat current via a Poiseuille flow mechanism. With some sensitivity to its shortcomings (for example, watching that the collision rate thermalize the phonons) we have confidence in using the

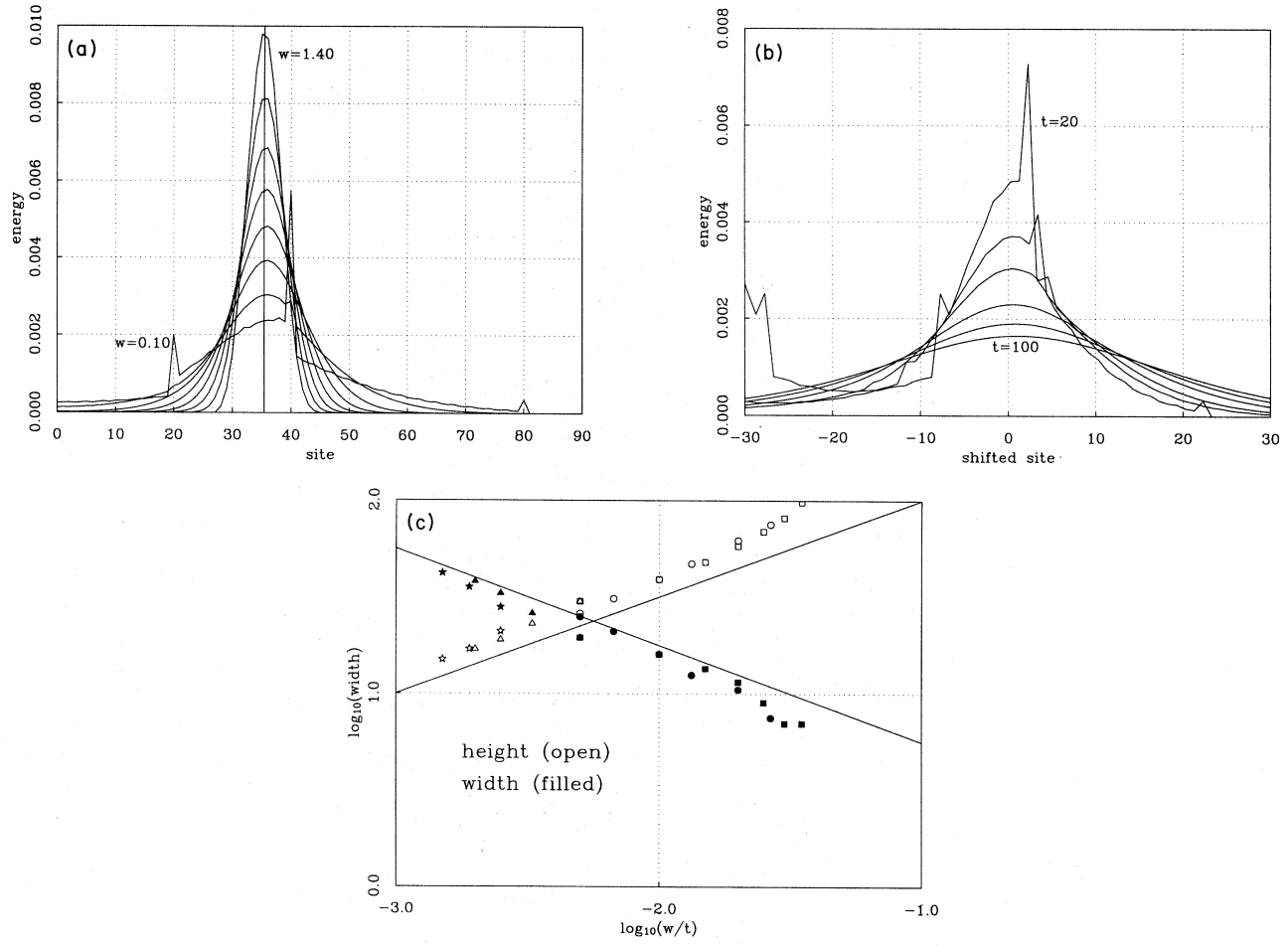

FIG. 4. Energy fluctuation as a function of position. For the conditions of example 2, $\beta_0=1, \beta=0.9, u=0$, the disturbance is at $\mathbf{x}=0$ at $t=0$. (a) The energy fluctuation is plotted as a function of site number at $t=40$ for values of the collision rate $w=0.1,0.2,0.4,0.6,0.8,1.0,1.2,1.4$. The vertical line at site 35 is the expected location of the second-sound pulse. (b) The energy fluctuation is plotted as a function of site number, collision rate $w=0.2$, for $t=20,30,40,60,80,100$. Each of the six curves has been shifted back toward the origin by the distance the disturbance would propagate as a second-sound pulse. In (c) the pulse height (open symbols) and half-width (filled symbols) are plotted as a function of $\eta t \propto t/w$ for a variety of conditions: stars ($w=0.15, t=60,80,100$), triangles ($w=0.2, t=40,60,80,100$), circles ($w=0.4, t=15,20,30,40,60,80$), squares ($w=0.2,0.4,0.6,0.8,1.0,1.2,1.4, t=40$). The two solid lines are guides to the eye of slope ± 0.5.

LBA to do experiments on the phonon gas away from the circumstances that let us anticipate its behavior. However, before going on we back up to look at the collision operator and the relaxation time approximation.

In Sec. III in trying to give a sound analytic demonstration that the computational rules reduced in appropriate limits to hydrodynamics we started with the exact phonon collision operator. We were turned away from just plugging ahead when we saw that the null space of the collision operator had more modes than there were conserved quantities. This meant that a pathological hydrodynamics might (certainty would?) result. We adopted the relaxation time approximation to avoid difficulties we did not know how to handle. To illustrate what was going on let us look at the behavior of a LBA that uses the exact collision operator in place of the relaxation time approximation. Thus we take the system to be described by Eq. (2) and Eqs. (3) and (4).

Example 3. At $\beta_0=1, \mathbf{u}=\mathbf{0}, w=0.1$ we perturb the system at $x=0$ at $t=0$ with $\beta=0.9$. In Fig. 5 we show the amplitude of the energy perturbation as a function of position for $t=10$, 20, 40, and 80. This figure should be compared to Figs. 3(a) and 3(b). The comparison is striking. We see the second-sound mode being assembled almost where it should be. The second-sound mode travels at almost the right speed, broadens as it travels further, etc. as we have come to expect. [As in Figs. 3(a) and 3(b) the filled boxes are the expected location of the second-sound mode.] However, we also see an energy spike at $x=c_T t$ that does not go away. Once established this feature translates at velocity c_T without further change. This feature is the evidence of the presence in the operation of the LBA of the pathological states that are in the null space of the collision operator. It was our unwillingness to have these states present or to remove them by artificial means that led us to retreat from the exact collision operator to the relaxation time approximation.

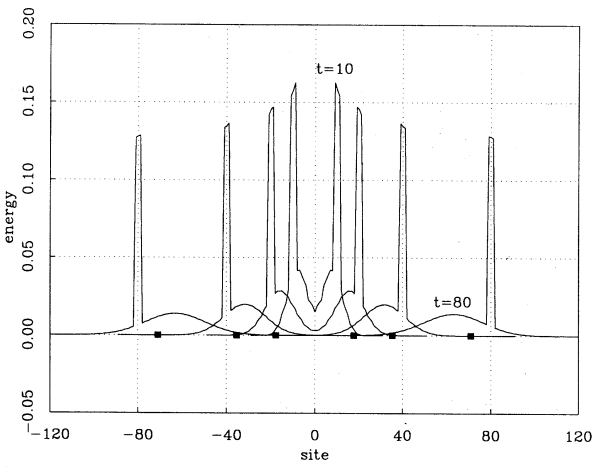

FIG. 5. Pathological energy propagation. The energy fluctuation is plotted as a function of site for the conditions of example 3; $\beta_0=1, \beta=0.9, u=0, w=0.1$, the disturbance is at $\mathbf{x}=\mathbf{0}$ at $t=0$. The four curves correspond to $t=10,20,40,80$. The initial disturbance is propagated according to the computational rule that includes exact treatment of the phonon collision operator. These results should be compared to those in Fig. 3 that result from use of the relaxation time approximation. The filled squares show the expected location of a second-sound pulse.

Now let us look at the phonon gas in more trying circumstances. As a first example we consider two extreme cases of energy pulse propagation: (a) near-ballistic pulse propagation because of weak phonon-phonon collisions and (b) near-"shock" pulse propagation because of strong phonon-phonon collisions and large initial disturbance.

Example 4(a). At $\beta_0=1, \mathbf{u}=\mathbf{0}$, we perturb the system at $x=0$ at $t=0$ with $\beta=0.9$. We look at $t=40$ as we let the collision rate vary from very weak, $w=0.05$, to reasonably strong, $w=0.60$. The results are shown in Fig. 6(a). At the lowest collision rates ballistic phonons are seen at sites 20, 40, and 80. There also are pronounced backgrounds: (1) longitudinal phonons from the location of the furthest forward longitudinal phonon at $x=0.80$ to the region of excess transverse phonons at $x=40$ and (2) transverse phonons at $x<40$. The fundamental events taking place to cause the evolution of the initial disturbance are collisions of the phonons in the energy fluctuation with the phonon in the ambient phonon gas. As the collision rate is increased, the dominant phonons, the ambient transverse phonons, exert their influence on the phonons in the energy perturbation and assemble them into a temperature pulse. The vertical line near site 35 in the figure is the expected location for a second-sound pulse.

It is the ambient phonons that work through the collision process to assemble the energy perturbation into a second-sound pulse. This process works well when there are lots of ambient phonons, compared to the number in the energy perturbation, and when the collision rate between these two groups of phonons is large. What happens as the size of the energy perturbation is increased?

Example 4(b). At $\beta_0=1, \mathbf{u}=\mathbf{0}$, we perturb the system at $x=0$ at $t=0$ with $\beta=0.1$. (The initial temperature disturbance is ten times as large as the ambient temperature.) For two large values of the collision rate, $w=1.0$ and 1.75, we look at the energy perturbation as a function of time, $t=10,\ldots,70$. See Fig. 6(b). We use relatively large values of w so that the energy perturbation will retain its integrity as it moves. Even for the largest w the energy perturbation is down to roughly one-half of the ambient energy at $t=10$. For both $w=1.0$ and 1.75 the energy pulse has a sharp front edge early in time; it is an incipient shock pulse. The dramatic influence of the collision rate is seen as the pulse travels. The pulse does not develop into a shock wave but is slowly rounded and degraded toward second-sound pulse appearance. This evolution is complete for the $w=1$ pulses by $t\approx 50$. It still has some way to go at $t=70$ for the $w=1.75$ pulses.

In the limit of low collision rate or for large-amplitude disturbances it is difficult to follow the evolution of the phonon gas by analytic means. The advantage of the LBA is apparent.

As a second example of use of the LBA to examine the behavior of the phonon gas we consider the experimental situation discussed by Coleman and co-workers [7]. We want to examine the behavior of an energy perturbation in the presence of a steady heat current.

Example 5. We establish an ambient phonon gas that has uniform temperature, $\beta_0=1$, and carries a steady heat current from left to right. The strength of this heat current is varied from 0 to $|v_0|=0.40$. We fix the collision rate at $w=0.2$. At $t=0$ at $x=0$ we introduce an energy perturbation, $\beta=0.9$. This energy perturbation has been carefully designed so as not to introduce net momentum into the phonon gas. We study the propagation of this energy perturbation upstream (against the steady heat current, i.e., to the left) and downstream (with the steady heat current, i.e., to the right). The results are shown in Figs. 6(a) and 6(b). In this figure the energy perturbation at $t=100$ is shown, $0.0\le v_0\le 0.40$. At $v_0=0$ the energy perturbation is well established as a second-sound pulse. Recall $w=0.2$. As v_0 is increased, causing a heat current to flow to the right, the right hand going temperature pulse is pushed more rapidly to the right, seemingly toward the velocity of the transverse phonons. The left hand going pulse is slowed by the heat current against which it is moving. The left hand going pulse is much more noticeably influenced by the heat current than the right hand going pulse. (The heat current values used here become unphysical at $v_0>0.1$. To illustrate matters of principle we use values of v_0 larger than 0.1.)

A first conclusion is possible.

(1) Coleman and co-workers show that a heat current will propagate against the uniform flow more rapidly than it will propagate with the flow. This prediction is

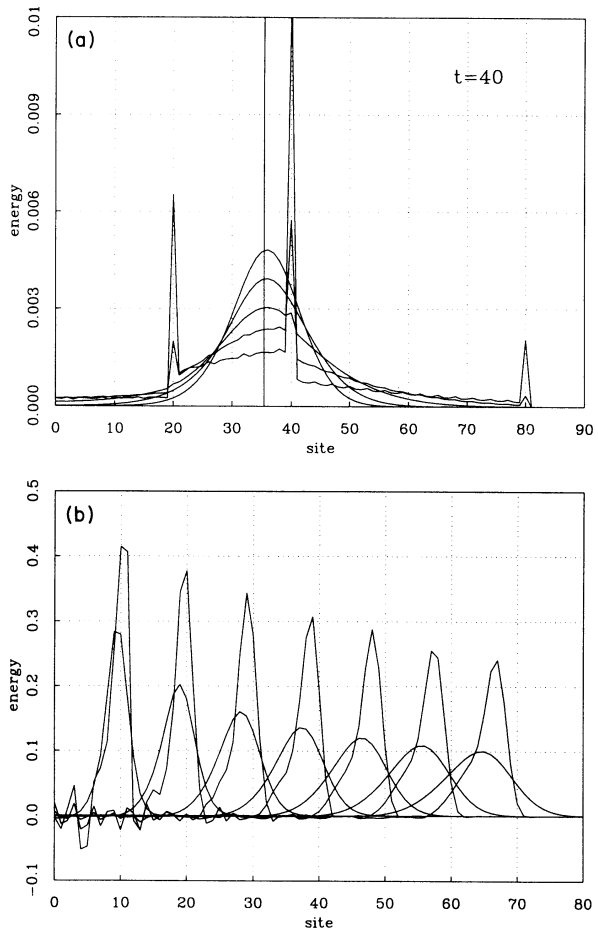

FIG. 6. Nonlinear energy fluctuations. In (a) the energy fluctuation is plotted as a function of site for the conditions of example 4(a); $\beta_0=1$, $\beta=0.9$, $u=0$, and $t=40$. The collision rate varies from 0.05 to 0.04; 0.05,0.10,0.20,0.30,0.40. The expected location of the second-sound pulse is indicated by the vertical line. In (b) the $\beta=0.1$ energy fluctuation is plotted for seven values of the time, $t=10$, 20, 30, 40, 50, 60, and 70. The initial conditions are those of example 4(a); $\beta_0=1,\beta=0.1,u=0$, the disturbance is at $\mathbf{x}=\mathbf{0}$ at $t=0$. Results for two values of the collision rate are shown; the taller curve at each time corresponds to $w=1.75$, the shorter curve at each time corresponds to $w=1.0$. (Because of the choice of length scale and time scale an energy pulse in flight for 40 time units is near site 40.) Compare the energy scale here with that in other examples, e.g., Fig. 3; the initial disturbance used here is very large. The collision rates used here are also very large so that the energy pulse retains its integrity and the evolution of "shocklike" features can be followed.

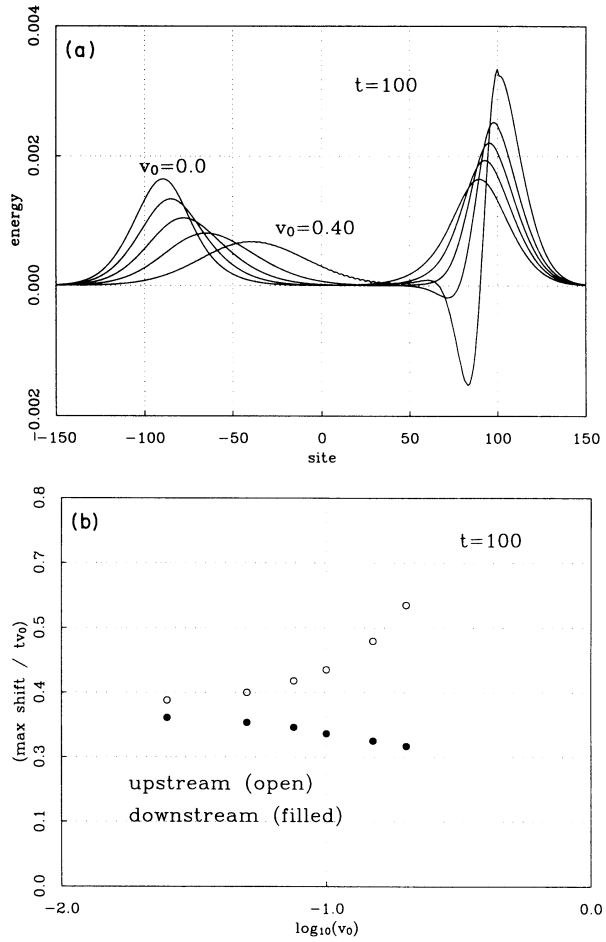

FIG. 7. Energy fluctuation as a function of position with $u\neq 0$. For the conditions of example 5, $\beta_0=1,\beta=0.9,w=0.2$, the disturbance is at $\mathbf{x}=\mathbf{0}$ at $t=0$. (a) The energy fluctuation as a function of site at $t=100$ for $v_0=0,0.1,0.2,0.3,0.4$. In (b) the shift in the position of the left and right hand going pulses from (a) is shown as a function of v_0 in the form of (shift in position of the pulse maximum)/$v_0 t$.

contrary to what we observe.

(2) As v_0 is increased we see that the right hand going energy perturbation becomes steeper and acquires shock-like features.

In Fig. 7 we show the behavior of the drift velocity of the right hand and left hand pulses as a function of v_0. The points plotted in this figure are the location of the maximum of the energy perturbation. To make it clear that the energy perturbation drifts with the ambient heat current we have plotted the ratio (shift in the position of the maximum in the energy perturbation)/$v_0 t$ against v_0. It is clear that only at the most modest values of v_0 is the drift velocity strictly proportional to v_0. Nonlinear effects show up at values of v_0 of order 0.10. The value of the drift velocity found by this simple analysis of the maximum in the energy fluctuation is (drift velocity)$\approx 0.4 v_0$. The result in Eq. (B17) yields (drift velocity)$\approx 0.5 v_0$. Given the crudeness of our analysis of the data we regard this agreement as reasonable.

In this section we have looked at several examples of the use of the LBA to see the behavior of the phonon gas. Two of these examples let us establish that the LBA reliably reproduced the hydrodynamics of the phonon gas. Two of them let us illustrate use of the LBA to look at phenomena that are not easily examined by analytical means.

V. CONCLUSION

In this paper we have developed and employed a lattice Boltzmann computational apparatus for numerical studies of the phonon gas. This LBA describes a phonon gas with two phonon polarizations that interact through energy and momentum conserving three-phonon collisions, i.e., cubic anharmonicity. Prior to employing the LBA we demonstrated that in suitable approximation the computational rules led to the known equations of phonon hydrodynamics. In carrying through this demonstration we encountered problems with the three-phonon collision operator. Our interest is in the phonon gas both in the strong collision limit, when it is described by a Navier-Stokes equation, and in the weak collision limit, when ballistic phonons are present. To handle this broad range of conditions simply we modified the three-phonon collision rules, replacing them by a relaxation time approximation. It is the resulting computational rules that reduced, for slowly varying long wavelength disturbances, to linear phonon hydrodynamics in relaxation time approximation.

To confirm that the computational rules were working well we studied the behavior of the second-sound mode, the fundamental mode of the linearized phonon hydrodynamics. We used the computational rules to follow the propagation of weak temperature disturbances. These disturbances, temperature pulses that started at the origin, were found to translate at constant velocity, i.e., they were a superposition of nondispersive temperature waves. Their velocity was in agreement with the prediction of the linear phonon hydrodynamics for the second-sound mode. In addition we studied the evolution of the structure of the temperature pulse and confirmed that the computational rules reliably described the effect of the phonon viscosity.

We studied the phonon gas, using the computational rules, in three examples in which the phonon gas was well away from the conditions appropriate to linearized phonon hydrodynamics; (1) in the limit of weak phonon-phonon collisions, (2) in the limit of strong collisions and nonperturbative temperature disturbances (i.e., in near-shock conditions), and (3) for a perturbative temperature fluctuation in the presence of a steady heat current. These computer experiments were primarily intended to illustrate the power of the LBA in describing the phonon gas for a broad range of conditions.

The third example was chosen to test the interesting prediction for behavior of a temperature pulse by Coleman and co-workers. For this case we regard the result of running the LBA as the result of the relevant experiment. We found, in disagreement with Coleman and co-workers, that the temperature pulse moved more rapidly in the direction of the heat current than it did against the heat current. Treatment of this circumstance with the appropriate extension of linear phonon hydrodynamics confirms this experimental finding and confirms the size of the shift in second-sound speed. The results of Coleman and co-workers result from a set of equations that are qualitatively different from those we find, see Appendix B. In particular, Coleman and co-workers use an energy conservation equation, developed to second order, in conjunction with a heat current equation, the Cattaneo equation, that is first order. Both the energy equation and the heat current equation in Appendix B have important second order terms.

The set of computational rules we have used to construct a LBA for the phonon gas lend themselves easily to generalization to more complex circumstances. We present the following examples.

(1) Phonon collision processes that do not conserve momentum, e.g., scattering from impurities or umklapp scattering, are accounted for by an additive collision operator (or relaxation time) that does not conserve momentum.

(2) Phonon motion through a complex environment, as in a crystal with boundaries, is handled with a mask that keeps track of hexagons in inaccessible regions of space.

It is apparent that the method discussed here for the two component phonon gas could also be used, with slight modification, to describe the phonon-roton gas in liquid ^{4}He and a variety of similar systems. The LBA developed here should let us do experiments on models of a variety of physical systems that will broaden our understanding of these systems and enhance their usefulness as a testing ground of principles and as a tool for investigation.

APPENDIX A: THE COLLISION OPERATOR

The phonon collision operator appropriate to the processes shown in Fig. 2 is

$$\left[\frac{\partial M_i}{\partial t}\right]_c = \frac{W_i^0[M,N]}{w\Delta t}$$
$$= N_{i-1}(1+M_i)(1+M_{i-2}) + N_{i+1}(1+M_i)(1+M_{i+2}) - M_i M_{i-2}(1+N_{i-1}) - M_i M_{i+2}(1+N_{i+1}) , \quad \text{(A1)}$$

$$\left[\frac{\partial N_i}{\partial t}\right]_c = \frac{W_i^1[M,N]}{w\Delta t}$$
$$= M_{i+1}M_{i-1}(1+N_i) - N_i(1+M_{i+1})(1+M_{i-1}) . \quad \text{(A2)}$$

For $M=P_0$ and $N=Q_0$, $W_i^0[P_0,Q_0]=0$ and $W_i^1[P_0,Q_0]=0$. Linearizing W in terms of departure from strict equilibrium, i.e., in terms of $\Delta M = M - P_0$ and $\Delta N = N - Q_0$ we find

$$W_i^0[\Delta M,\Delta N] = w\Delta t[A_{01}(\Delta N_{i+1}+\Delta N_{i-1}) - A_{00}(\Delta M_{i+2}+2\Delta M_i+\Delta M_{i-2})] \quad \text{(A3)}$$

and

$$W_i^1[\Delta M,\Delta N] = w\Delta t[-A_{11}\Delta N_i + A_{10}(\Delta M_{i+1}+\Delta M_{i-1})], \quad \text{(A4)}$$

where

$$A_{00} = A_{10} = P_0 - Q_0 \quad \text{(A5)}$$

and

$$A_{01} = A_{11} = 1+2P_0 . \quad \text{(A6)}$$

This operator can be written in the form

$$W_{ij}^{\sigma\sigma'} = w\Delta t A_{\sigma\sigma'}\Delta_{ij}^{\sigma\sigma'} , \quad \text{(A7)}$$

where

$$\Delta_{ij}^{00} = \delta_{j,i+2}+2\delta_{j,i}+\delta_{j,i-2} ,$$
$$\Delta_{ij}^{01} = \Delta_{ij}^{10} = -(\delta_{j,i+1}+\delta_{j,i-1}) , \quad \text{(A8)}$$
$$\Delta_{ij}^{11} = \delta_{j,i} .$$

Because the off diagonal terms are unequal, $A_{01}\neq A_{10}$, the operator W is not symmetric in $i,\sigma\leftrightarrow j,\sigma'$. W is symmetrized by using $\Delta M = \Delta m/\sqrt{A_{00}}$, and $\Delta N = \Delta n/\sqrt{A_{11}}$. We denote Δm and Δn by $\Delta r^\sigma, \sigma=0,1$ corresponding to m,n, respectively.

In terms of the symmetrized collision operator the right hand side of the linearized Boltzmann equation is

$$\sum_{j,\sigma'} \mathcal{C}_{ij}^{\sigma\sigma'}\Delta r_j^{\sigma'} , \quad \text{(A9)}$$

where

$$\frac{\mathcal{C}_{ij}^{\sigma\sigma'}}{w\Delta t} = a_{\sigma\sigma'}\Delta_{ij}^{\sigma\sigma'} , \quad \text{(A10)}$$

with

$$a_{00} = A_{00} ,$$
$$a_{01} = a_{10} = \sqrt{A_{00}A_{11}} , \quad \text{(A11)}$$
$$a_{11} = A_{11} .$$

The eigenvalue problem associated with $\mathcal{C}$ is solved by standard methods. Use

$$\psi_\nu(m,\sigma) = b_\sigma e^{i\nu m} , \quad \text{(A12)}$$

$m=1,2,\ldots,6$ with ν such that $\psi_\nu(m+6,\sigma)=\psi_\nu(m,\sigma)$. There are 12 eigenvalues. Six of these are nonzero and six are zero. The six nonzero eigenvalues are twofold and fourfold degenerate:

$$\lambda_\nu = a_{11}+4a_{00} \quad \text{(twofold)} ,$$
$$\lambda_\nu = a_{11}+a_{00} \quad \text{(fourfold)} .$$

The null space contains six vectors. These vectors correspond to the three states that represent conservation laws (energy, x momentum, and y momentum) and to three pathological states. These six vectors corresponding to $\lambda_\nu=0$ constitute the null space of the collision operator. The vectors associated with the conservation laws are found from Eq. (A9) upon considering the case in which Δr^σ is a local equilibrium fluctuation away from strict equilibrium. In addition to these three vectors there are three vectors in the null space that represent highly nonuniform equilibrium distributions. It is these latter vectors that are responsible for the difficulties remarked on in Sec. III and illustrated in Sec. IV.

APPENDIX B: CONSERVATION LAWS

In this appendix we sketch explicit calculation of (1) the local equilibrium densities, (2) the average energy and the average momentum, and (3) the energy and momentum conservation laws. We do this in terms of the local equilibrium variables. At the very end we also write out the conservation laws in terms of the local hydrodynamic variables.

(1) The local equilibrium densities are defined to be $N(\xi_\sigma)$, Eqs. (5) and (6), where

$$\xi_\sigma = x_\sigma(1+\delta\alpha) - x\mathbf{e}\cdot\mathbf{v}(1+\delta\alpha) , \quad \text{(B1)}$$

$N(x)=1/(e^x-1)$, and

$$x = \beta_0\epsilon ,$$
$$x_\sigma = \beta_0\epsilon_\sigma ,$$
$$\mathbf{v}(1) = \frac{\mathbf{u}(1)}{c} ,$$
$$\delta\alpha(1) = \frac{\beta(1)-\beta_0}{\beta_0} .$$

(2) The average energy and average momentum are defined by

$$\beta_0 e(1)=\sum_{i,\sigma} x_\sigma N(\xi_\sigma) , \tag{B2}$$

$$\frac{p_x(1)}{p}=\sum_{i,\sigma} (\mathbf{e}_i)_x N(\xi_\sigma) , \tag{B3}$$

with $N(\xi_\sigma)$ given by Eq. (B1).

(3) The energy and momentum conservation laws are

$$\sum_{i\sigma} \epsilon_\sigma \frac{\partial}{\partial t} N(\xi_\sigma)+\sum_{i\sigma} \epsilon_\sigma c_\sigma \mathbf{e}_i\cdot\nabla N(\xi_\sigma)=0 , \tag{B4}$$

$$\sum_{i\sigma} \frac{\partial}{\partial t} N(\xi_\sigma)+\sum_{i\sigma} (\mathbf{e}_i)_x c_\sigma \mathbf{e}_i\cdot\nabla N(\xi_\sigma)=0 . \tag{B5}$$

These quantities are found to desired order in the small quantities, $\delta\alpha(1)$ and $\mathbf{v}(1)$, by developing $N(\xi_\sigma)$ in Taylor series in $\xi_\sigma - x_\sigma$. We illustrate here the case in which the drift velocity has a steady component, $\mathbf{v}_0$, as well as a fluctuating component, $\delta\mathbf{v}(1)$. We treat terms of first order smallness, $\delta\alpha, \delta\mathbf{v}, \mathbf{v}_0$, and of second order smallness, $\mathbf{v}_0\cdot\mathbf{v}_0, \mathbf{v}_0\delta\alpha, \mathbf{v}_0\cdot\delta\mathbf{v}$. Terms of second order in the fluctuating fields, $\delta\alpha^2$ and $\delta\mathbf{v}\cdot\delta\mathbf{v}$, are ignored. We imagine the steady component of the drift velocity is established by suitable means. The ambient conditions of the phonon gas are $\delta\alpha=0$ and $\mathbf{v}=\mathbf{v}_0$. Perturbations away from these ambient conditions are described by the fields, $\delta\alpha$ and $\delta\mathbf{v}$. Finally to keep x, in and below Eq. (B1), from being confused with a direction x we take the $\mathbf{e}_1$ direction to be z; we specialize to one-dimensional motion along the z axis; $\mathbf{v}_0 \propto \mathbf{e}_1$.

(1) For $N(\xi_\sigma)$ we find

$$\begin{aligned} N(\xi_\sigma)-N_{\text{ambient}} = &-x_\sigma N'_\sigma \delta\alpha + x^2 N''_\sigma \mathbf{e}\cdot\mathbf{v}_0 \mathbf{e}\cdot\delta\mathbf{v} \\ &- xN'_\sigma(\mathbf{e}\cdot\delta\mathbf{v}+\mathbf{e}\cdot\mathbf{v}_0\delta\alpha) \\ &- xx_\sigma N''_\sigma \mathbf{e}\cdot\mathbf{v}_0\delta\alpha , \end{aligned} \tag{B6}$$

with

$$N_{\text{ambient}}=N(x_\sigma)-xN'_\sigma \mathbf{e}\cdot\mathbf{v}_0+\frac{x^2}{2}N''_\sigma(\mathbf{e}\cdot\mathbf{v}_0)^2 , \tag{B7}$$

$N'_\sigma = \partial N(x_\sigma)/\partial x_\sigma$, and $N''_\sigma = \partial N'_\sigma/\partial x_\sigma$.

(2) Using Eqs. (B6) and (B7) we calculate the energy and momentum as called for in Eqs. (B2) and (B3) and find

$$\beta_0 \Delta e(1)=F_3\delta\alpha(1)+\tfrac{1}{2}G_2 v_0 \delta v(1) , \tag{B8}$$

$$\Delta p_z(1)=-\frac{p}{2}\{F_1[\delta v(1)+v_0\delta\alpha(1)]+G_1 v_0\delta\alpha(1)\} , \tag{B9}$$

where $\Delta e(1)$ and $\Delta p_z(1)$ are the departures of the energy and momentum from the ambient values. The constants $F_1, \ldots, G_4$ appearing here and below are defined and discussed further along in this appendix.

(3) Using Eq. (B6) in Eqs. (B4) and (B5) for energy and momentum conservation we find

$$\frac{\partial}{\partial t}\left[\delta\alpha+\frac{G_2}{2F_3}v_0\delta v\right]-\frac{c}{2}\frac{\partial}{\partial z}\left[\delta v+\left[1+\frac{G_4}{F_4}\right]v_0\delta\alpha\right]=0 \tag{B10}$$

and

$$\frac{\partial}{\partial t}\left[\delta v+\left[1+\frac{G_1}{F_1}\right]v_0\delta\alpha\right]=\frac{cF_3}{xF_1}\frac{\partial}{\partial z}\left[\delta\alpha+\frac{3G_2}{4F_3}v_0\delta v\right] =0 . \tag{B11}$$

The coefficients in Eqs. (B8)–(B11) are

$$F_1=6x(P'_0+Q'_0) ,$$

$$F_2=6x\left[\frac{P'_0}{2}+Q'_0\right] ,$$

$$F_3=6x^2\left[\frac{P'_0}{4}+Q'_0\right] ,$$

$$G_1=6x^2\left[\frac{P''_0}{2}+Q''_0\right] ,$$

$$G_3=6x^3\left[\frac{P''_0}{4}+Q''_0\right] ,$$

$$G_4=6x^4\left[\frac{P''_0}{8}+Q''_0\right] ,$$

$$F_4=xF_3 ,$$

$$G_2=xG_1 ,$$

$$G_0=\frac{G_4}{x} .$$

We define

$$\mathcal{E}=-\left[\delta\alpha+\frac{G_2}{2F_3}v_0\delta v\right] \tag{B12}$$

and

$$\mathcal{P}=\delta v+\left[1+\frac{G_1}{F_1}\right]v_0\delta\alpha \tag{B13}$$

and write the conservation laws in the form

$$\frac{\partial\mathcal{E}}{\partial t}+\lambda_E u_0\frac{\partial\mathcal{E}}{\partial z}+\frac{c}{2}\frac{\partial\mathcal{P}}{\partial z}=0 \tag{B14}$$

and

$$\frac{\partial\mathcal{P}}{\partial t}+\lambda_P u_0\frac{\partial\mathcal{P}}{\partial z}+c\chi\frac{\partial\mathcal{E}}{\partial z}=0 , \tag{B15}$$

where

$$\lambda_E=\frac{1}{2}\left[\frac{G_4}{F_4}-\frac{G_1}{F_1}\right] ,$$

$$\lambda_P=-\frac{G_2}{4xF_1} ,$$

$\chi=F_3/xF_1$ and $u_0=v_0/c$. The energy $\mathcal{E}$ and momentum $\mathcal{P}$ are linear in the fluctuating fields. Thus from Eqs. (B14) and (B15) we can find the velocity of small-amplitude fluctuations; (1) $[v_0=0]$:

$$\frac{\omega^2}{k^2c^2}=\frac{F_3}{2xF_1} . \tag{B16}$$

This is the equation for the velocity of second sound. (2) [$\mathbf{v}_0\neq\mathbf{0}$]:

$$\frac{\omega}{kc}=\pm\left[\frac{F_3}{2xF_1}\right]^{1/2}+\frac{\lambda_E+\lambda_P}{2}v_0 . \tag{B17}$$

This equation shows that a second-sound pulse moving to the left or right will have a drift velocity in a direction that depends on the sign of v_0 and the sign of $\lambda_E+\lambda_P$. We find $\lambda_E+\lambda_P>0$ for all x from numerical or analytical study of the behavior of $F_1,\ldots,G_4$. Thus for $v_0>0$, a steady heat current to the right, a second-sound pulse will move more slowly to the left (upstream) than it will to the right (downstream).

For completeness we write out the conservation laws to second order in the hydrodynamic variables, $\Delta e(1)$ and $\Delta\mathbf{p}(1)$. They are

$$\frac{\partial\Delta e}{\partial t}+c_L\chi\nabla\cdot\Delta\mathbf{p}+c_L\Lambda_e\nabla\cdot(\Delta e\,\Delta\mathbf{p})=0 \tag{B18}$$

and

$$\frac{\partial\Delta\mathbf{p}}{\partial t}+\frac{c_L}{2}\chi\nabla\cdot\Delta e+\frac{c_L}{2}\Lambda_p(\nabla\cdot\Delta\mathbf{p})\Delta\mathbf{p}=0 , \tag{B19}$$

where Δe and Δp have been normalized by ϵ and p, respectively, and

$$\Lambda_e=\frac{1}{F_1}\left[\frac{G_0}{F_3}-\frac{G_1}{F_1}\right] \tag{B20}$$

and

$$\Lambda_p=\frac{G_1}{F_1^2} . \tag{B21}$$

[1] See, for example, D. Forster, *Hydrodynamic Fluctuations, Broken Symmetry and Correlation Functions* (Benjamin, Reading, MA, 1975).

[2] R. A. Guyer and J. A. Krumhansl, Phys. Rev. **148**, 766 (1966); **148**, 778 (1966).

[3] C. C. Ackerman, B. Bertman, H. A. Fairbank, and R. A. Guyer, Phys. Rev. Lett. **16**, 789 (1966).

[4] C. C. Ackerman and W. C. Overton, Phys. Rev. Lett. **22**, 764 (1969).

[5] C. C. Ackerman and R. A. Guyer, Ann. Phys. (N.Y.) **50**, 128 (1968).

[6] H. E. Jackson, C. T. Walker, and T. F. McNelly, Phys. Rev. Lett. **25**, 26 (1970); V. Narayanamurti and R. C. Dynes, *ibid.* **28**, 1461 (1972).

[7] B. D. Coleman, M. Fabrizio, and D. R. Owen, Rend. Semin. Mat. Univ. Padova **68**, 207 (1982).

[8] C. Cattaneo, Atti Semin. Mat. Fis. Univ. Modena **3**, 83 (1948).

[9] *Kinetic Theory and Extended Thermodynamics,* edited by I. Muller and T. Ruggeri (Pitagora, Bologna, 1987); I. Muller and T. Ruggeri, *Extended Thermodynamics* (Springer-Verlag, New York, 1993); T. Ruggeri, A. Muracchini, and L. Seccia (unpublished).

[10] G. Doolen, *Lattice Gas Methods* (Addison-Wesley, Redwood City, CA, 1990).

[11] J. N. Kapur and H. K. Kesavan, *Entropy Optimization Principles with Applications* (Academic, New York, 1992).

[12] N. W. Ashcroft and N. D. Mermin, *Solid State Physics* (Holt, Rinehart and Winston, New York, 1976).